ACS APPLIED MATERIALS & INTERFACES

Research Article

www.acsami.org

Improved Cycle Stability and Rate Capability of Graphene Oxide Wrapped Tavorite $LiFeSO_4F$ as Cathode Material for Lithium-Ion Batteries

Zhendong Guo,[†] Dong Zhang,*[,†] Hailong Qiu,[†] Tong Zhang,[†] Qiang Fu,[†] Lijie Zhang,[†] Xiao Yan,[§] Xing Meng,[†] Gang Chen,[†,‡] and Yingjin Wei*[,†]

[†]Key Laboratory of Physics and Technology for Advanced Batteries (Ministry of Education), College of Physics and [‡]State Key Laboratory of Superhard Materials, Jilin University, Changchun 130012, P. R. China

[§]CAS Key Laboratory of Biobased Materials, Qingdao Institute of Bioenergy and Bioprocess Technology, Chinese Academy of Sciences, Qingdao 266101, P. R. China

Supporting Information

ABSTRACT: Tavorite $LiFeSO_4F$ has been regarded as a promising alternative to $LiFePO_4$ due to its high Li ionic conductivity. To overcome the low electronic conductivity of $LiFeSO_4F$, we prepared a graphene oxide (GO)/$LiFeSO_4F$ composite material by the solvothermal method. The GO wraps on the surface of $LiFeSO_4F$ and links the adjacent particles, thus providing an effective network for electrons transport. As a result, the electronic conductivity of the material is improved from 8.16×10^{-11} S cm^{-1} to 1.65×10^{-4} S cm^{-1}. In addition, the GO depresses the side reactions of the electrode and electrolyte, promotes the charge transfer reactions at the electrode/electrolyte interface, and facilitates the lithium diffusion in the electrode. The GO-wrapped $LiFeSO_4F$ exhibits much better electrochemical performance than the pristine material. It showed a discharge capacity of 113.2 mAh g^{-1} at the 0.1 C rate with 99% capacity retention after 100 cycles. In addition, the material is able to deliver 85.1, 73.4, and 30.3 mAh g^{-1} at high current rates of 1 C, 2 C, and 10 C, respectively.

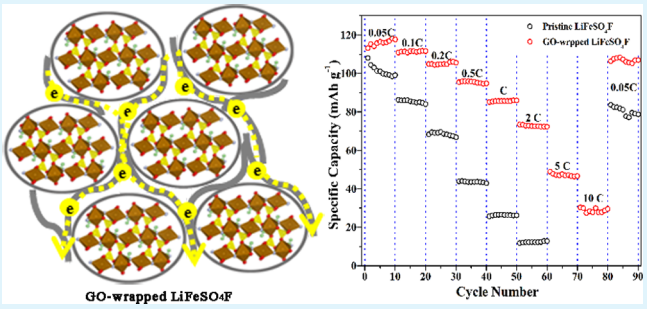

KEYWORDS: *lithium ion batteries, cathode material, lithium iron sulfate fluoride, graphene oxide, electrochemical performance*

1. INTRODUCTION

Li-ion batteries have been widely used in electrochemical energy storage because of their high energy densities and long cycle life. Increasing efforts are being dedicated to develop new cathode materials to replace the traditional layered $LiCoO_2$, which suffers from high cost, environmental hazard, and safety problems. Hence, several materials have been explored as potential alternatives, especially the polyoxyanion materials such as phosphates ($LiMPO_4$, M = Fe, Mn),[1] silicates (Li_2MSiO_4),[2] fluorophosphates (Li_2FePO_4F),[3] and borates ($LiMBO_3$).[4] These polyoxyanion materials exhibit higher working voltages and better safety properties than their corresponding oxide compounds such as $LiFeO_2$ and $LiMnO_2$. In particular, olivine $LiFePO_4$ has been considered as one of the most promising cathode materials for the emerging electric vehicles due to its low cost, low toxicity, and high safety. However, the one-dimensional Li diffusion pathway and intrinsic poor electronic conductivity of $LiFePO_4$ severely hinder the electrochemical performance of the battery.

In 2010, a new polyoxyanion cathode material, tavorite $LiFeSO_4F$, was first prepared by Tarascon et al. by the ionothermal method.[5] Although the material has a slightly lower theoretical capacity (151 mAh g^{-1}) than $LiFePO_4$, it shows a comparable specific energy to that of $LiFePO_4$ due to its higher discharge voltage. Recent computational works on the electronic structure, crystal structure, and ionic kinetic properties of tavorite $LiFeSO_4F$ have deeply revealed the electrochemical properties of this new cathode material.[6−8] It has shown that the framework of tavorite $LiFeSO_4F$ is built of two FeO_4F_2 octahedra linked by fluorine vertices in the *trans* position forming chains along the *c*-axis. The chains are bridged by isolated SO_4 tetrahedra, creating a three-dimensional framework and delimiting three tunnels along the [100], [010], and [101] directions. This open structure is very favorable for Li-ion transport. As has been reported, the Li ionic conductivity of tavorite $LiFeSO_4F$ is about three orders of magnitude higher than that of $LiFePO_4$, that is, 4×10^{-6} S cm^{-1} versus 2×10^{-9} S cm^{-1} at 147 °C.[5,9]

However, tavorite $LiFeSO_4F$ shows extremely low electronic conductivity of 5.2×10^{-11} S cm^{-1}, which is two orders of magnitude lower than that of olivine $LiFePO_4$.[5] This seriously hinders the electrochemical performance of the material

Received: April 6, 2015
Accepted: June 11, 2015
Published: June 11, 2015

DOI: 10.1021/acsami.5b02966
ACS Appl. Mater. Interfaces 2015, 7, 13972−13979

especially at high charge−discharge rates. Recently, some works used the solvothermal method, which is far more economical and scalable compared to the ionothermal method, to synthesize $LiFeSO_4F$.[10,11] However, the materials thus obtained showed very poor electrochemical performance, for example, only 30−40 mAh g^{-1} at the 0.2 C rate. To improve the electrochemical performance of the solvothermal prepared $LiFeSO_4F$, one should try to eliminate the residual organic contaminants or improve the electronic conductivity of the material. Carbon coating has been used for many years to improve the electronic conductivity of plyoxyanion cathode materials. Conventional carbon coating requires high temperature (>600 °C) for pyrolysis of organic compounds and an even higher temperature for carbonization. These techniques are not suitable for tavorite $LiFeSO_4F$ due to its low thermal decomposition temperature (450 °C). To improve the electronic conductivity, A. Sobkowiaket al. prepared poly(3,4-ethylenedioxythiophene) (PEDOT)-coated $LiFeSO_4F$ at low temperature.[12] The material showed improved rate capability and cycle stability. However, the preparation involved in a tedious multistep route and the reported discharge capacity, 50 mAh g^{-1} at the 2 C rate, is still too low for practical applications.

As an alternative strategy, the electronic conductivity of electrode materials can be tailored by combination with highly conductive carbonaceous materials such as carbon fibers,[13,14] carbon nanotubes,[15−17] mesoporous carbons,[18,19] and graphene oxide (GO),[20−22] etc. This method allows preparing target materials at mild temperatures by using hydrothermal or solvothermal reactions or at room temperature by using solve-mixing and ball-milling techniques. In this regard, it is very suitable for $LiFeSO_4F$, which cannot be prepared by conventional carbon coating techniques. In numerous carbonaceous materials, GO, which has high conductivity, large surface area, and excellent structural stability, has attracted particular attention. In general, GO in the composite electrode can act as both conductive channels and an elastic buffer to accommodate the volume change during repeated lithium uptake and removal, even at a low weight fraction. To the best of our knowledge, to date there is no work to study the electrochemical performance of $LiFeSO_4F$/carbon composite cathode. Herein, in this work we explored the possibility of using GO as a wrapping layer to improve the electrochemical performance of tavorite $LiFeSO_4F$.

2. EXPERIMENTAL SECTION

2.1. Synthesis of Tavorite $LiFeSO_4F$. Tavorite $LiFeSO_4F$ was prepared by a tetraethylene glycol (TEG) assisted solvothermal method. For the first step, $FeSO_4.H_2O$ was prepared by heating $FeSO_4.7H_2O$ at 100 °C for 3 h in an Ar/H_2 (93:7) atmosphere. The $FeSO_4.H_2O$ precursor was mixed with stoichiometric LiF and then ball-milled for 24 h in acetone. The mixture was transferred into a 43 mL Teflon-lined steel autoclave along with 30 mL of TEG. The autoclave was kept at 260 °C for 60 h to allow the solvothermal reaction. After it was cooled to room temperature naturally, the resulting white−gray powders were washed with acetone several times and then dried in vacuum-oven at 60 °C.

2.2. Synthesis of GO-Wrapped $LiFeSO_4F$. The GO suspension was prepared from natural graphite by a modified Hummers method, as reported elsewhere.[23] The GO-wrapped $LiFeSO_4F$ was prepared with the assistance of 3-aminopropyl-trimethoxysilane (APTMS). In detail, a certain amount of $LiFeSO_4F$ was dispersed in 100 mL of ethanol. Then, 10 mL of APTMS was added and refluxed at 80 °C for 4 h followed by sufficient washing with ethanol. Afterward, the APTMS-treated $LiFeSO_4F$ was added into the GO suspension with continuous stirring to ensure homogeneous mixing of $LiFeSO_4F$ and GO. The GO-wrapped $LiFeSO_4F$ was obtained after the powders were washed with ethanol several times.

2.3. Materials Characterizations. The crystal structures of the materials were studied by X-ray diffraction (XRD) on a Bruker AXS D8 diffractometer with Cu Kα radiation. The amount of GO in the material was determined by C/H/N elemental analysis using an ElementarVario EL cube. The morphologies of the materials were observed by scanning electron microscope (SEM, JSM-6700F) and transmission electron microscope (TEM, FEI Tecnai G2). Raman scattering was performed on a LabRAM HR Evolution system (Horiba Scientitle) using a 633 nm laser line. Fourier transform infrared spectroscopy (FTIR) was carried out on a Bruker Vertex80 V spectrometer with the samples loaded into a 300 μm hole in a T301 stainless-steel gasket, which was compressed in a diamond anvil cell. X-ray photoelectron spectroscopy (XPS) was performed on an ESCALAB spectrometer using Mg−Kα light source. For measurement of electronic conductivity, the samples were prepared to thin-film electrodes on an Al substrate with thickness of about 30 μm. Then, *dc* conductivity measurement was performed by the two-electrode method.

2.4. Electrochemical Measurements. The electrochemical experiments were conducted on CR2032-type coin cells using metallic lithium foil as the anode. The cathode was composed of 70 wt % active material, 20 wt % active carbon, and 10 wt % poly-vinylidenefluoride (PVDF) binder, which was pasted on an Al current collector. The anode and cathode were separated by Celgard 2400 membrane. A 1 mol L^{-1} lithium hexafluorophosphate ($LiPF_6$) solution dissolving in ethylene carbonate (EC) and diethyl carbonate (DEC) (EC/DEC = 1:1) was used as the electrolyte. Galvanostatic charge−discharge was performed on a LAND-2010 automatic battery tester in the voltage window of 2.5−4.5 V. Cyclic voltammetry (CV) and electrochemical impedance spectroscopy (EIS) were performed on a Bio-Logic VSP multichannel potentiostatic−galvanostatic system. The impedance data were recorded by applying an *ac* voltage of 5 mV in the frequency range from 1 MHz to 1 mHz.

3. RESULTS AND DISCUSSION

3.1. Structural and Physical Properties. Figure 1 shows the XRD patterns of the pristine and GO-wrapped $LiFeSO_4F$.

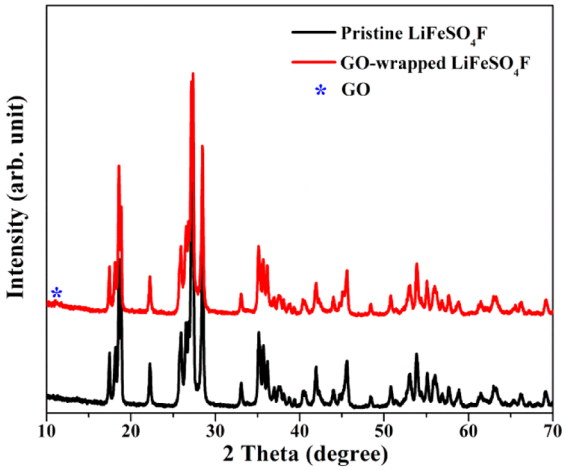

Figure 1. XRD patterns of the pristine and GO-wrapped $LiFeSO_4F$ materials.

The pristine sample shows the typical XRD pattern of tavorite $LiFeSO_4F$ without any possible impurities such as LiF and $FeSO_4$. The lattice parameters of the material are calculated to be a = 5.1848(3) Å, b = 5.5044(1) Å, c = 7.2321(1) Å, α = 106.558(5)°, β = 107.194(5)°, and γ = 97.775(3)°, which are in good agreement with those reported in the literature.[5,11] The

DOI: 10.1021/acsami.5b02966
ACS Appl. Mater. Interfaces 2015, 7, 13972−13979

XRD pattern of the GO-wrapped $LiFeSO_4F$ is almost identical to that of pristine $LiFeSO_4F$. The small peak at around 10.5° is characteristic of GO,[24] suggesting that GO is successfully incorporated with $LiFeSO_4F$. Elemental analysis shows that the amount of GO in the material is 1.77 wt %. The intensity of this peak becomes stronger with more GO added into the composite (Supporting Information, Figure S1). The existence of GO in the material is further confirmed by Raman scattering (Supporting Information, Figure S2). It was seen that the positions of the $LiFeSO_4F$-related Raman peaks (marked by * in the figure) are practically unchanged after incorporation with GO. However, the intensities of these Raman peaks are much weaker than those of pristine $LiFeSO_4F$. In addition, two strong peaks appear at 1356 and 1603 cm^{-1}, which are associated with the disordered (D) and graphitic (G) Raman bands of GO,[25] respectively.

SEM and TEM were used to obtain an insight into the morphological aspects of the samples. As seen from SEM (Figure 2a), the pristine sample is composed of submicron particles with polyhedral shape. The TEM (Figure 2b) image of $LiFeSO_4F$ shows an overwhelmingly clean surface. From the SEM image of the GO-wrapped $LiFeSO_4F$ (Figure 2c), it is evident that the GO layers are effectively wrapped on the outer surface of $LiFeSO_4F$. The fine structure of the GO-wrapped $LiFeSO_4F$ is further studied by TEM, as shown in Figure 2, panel d. In addition to the wrapping structure (red arrows), some GO films are seen to fill in the space of the material that effectively links the adjacent $LiFeSO_4F$ particles (blue arrows). Atomic force microscope shows that the GO has a two-dimensional feature with thickness about 1 nm, which is characteristic of monolayered GO (Supporting Information, Figure S3). During preparation of GO-wrapped $LiFeSO_4F$, the pristine $LiFeSO_4F$ was soaked in (3-aminopropyl)-trimethoxysilane (APTMS) to adsorb sufficient protons on the particle surface.[26] After the $LiFeSO_4F$ powders were mixed with GO suspension, the flexible GO self-wraps the $LiFeSO_4F$ particles as a result of the electrostatic interactions between the negative charges on GO and the positive charges on $LiFeSO_4F$. Hence, the GO constructs an effective percolating network as well as an increased intimate electronic contact area between different $LiFeSO_4F$ particles, which would significantly improve the electronic conductivity of the material. DC electronic conductivity measurement shows that the electronic conductivity of the pristine $LiFeSO_4F$ is 8.16×10^{-11} S cm^{-1}, which fits well with that reported in literature.[5] In contrast, the electronic conductivity of the GO-wrapped $LiFeSO_4F$ is increased to 1.65×10^{-4} S cm^{-1}, which is seven orders of magnitude higher than that of the pristine material.

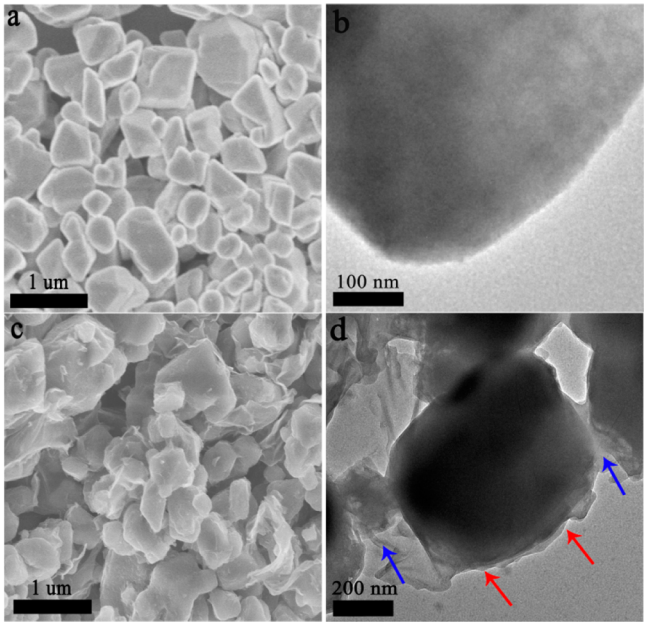

Figure 2. SEM and TEM images of (a, b) the pristine and (c, d) GO-wrapped $LiFeSO_4F$ materials.

The chemical states of the pristine and GO-wrapped $LiFeSO_4F$ were studied by XPS. Figure 3, panel a shows the Fe 2p XPS spectra of the materials. Both materials show two Fe 2p peaks at 711.3 and 724.8 eV, which correspond to the $2p_{3/2}$ and $2p_{1/2}$ binding energies of Fe^{2+}, respectively.[27] The C 1s XPS spectra of the materials are shown in Figure 3, panel b. The pristine $LiFeSO_4F$ shows a single C 1s XPS peak at 284.6 eV, which is assigned to carbon contamination (C═C/C−C) adsorbed on the surface of the product. The C 1s XPS spectra of GO-wrapped $LiFeSO_4F$ can be deconvoluted into four peaks, which are due to the C═C/C−C bond (284.6 eV) and some other functional groups including C−O (285.6 eV), C═O (287.4 eV), and COOH (288.9 eV),[28] respectively. Compared to the C 1s XPS of GO (Figure 3c), it was seen that the XPS peaks of these functional groups are significantly depressed. This indicates that the GO is partly reduced by the NH_2 group of APTMS.

3.2. Galvanostatic Charge−Discharge Performance.

Figure 4, panel a shows the first charge−discharge curves of the pristine $LiFeSO_4F$ and GO-wrapped $LiFeSO_4F$ in the voltage window of 2.5−4.5 V with a current density of 15 mA g^{-1} (0.1 C). Both materials show a pair of voltage plateaus at around 3.6

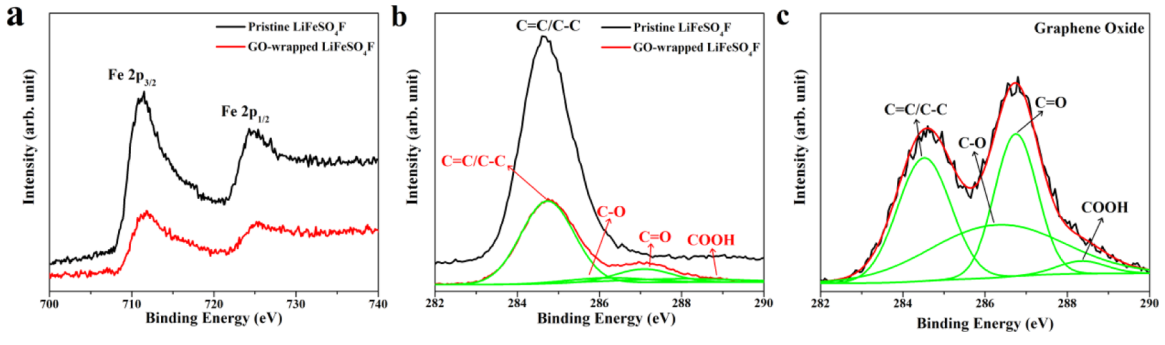

Figure 3. (a) Fe 2p and (b) C 1s XPS of the pristine and GO-wrapped $LiFeSO_4F$ materials; (c) C 1s XPS of GO.

DOI: 10.1021/acsami.5b02966
ACS Appl. Mater. Interfaces 2015, 7, 13972−13979

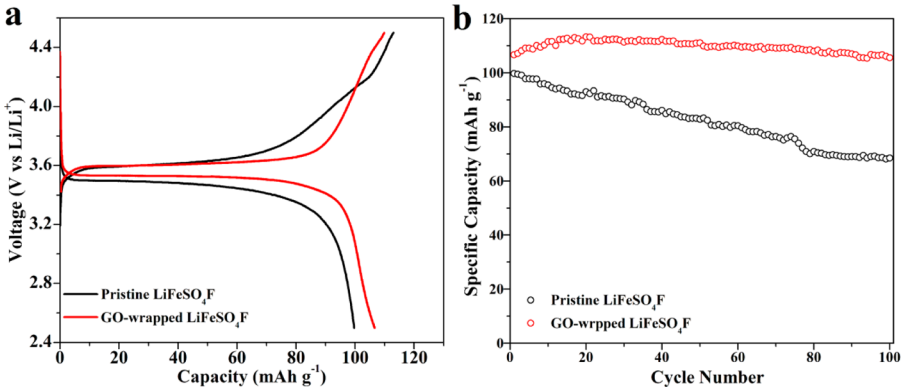

Figure 4. First (a) charge−discharge curves and (b) cycling performance of the pristine and GO-wrapped $LiFeSO_4F$ materials at the 0.1 C rate.

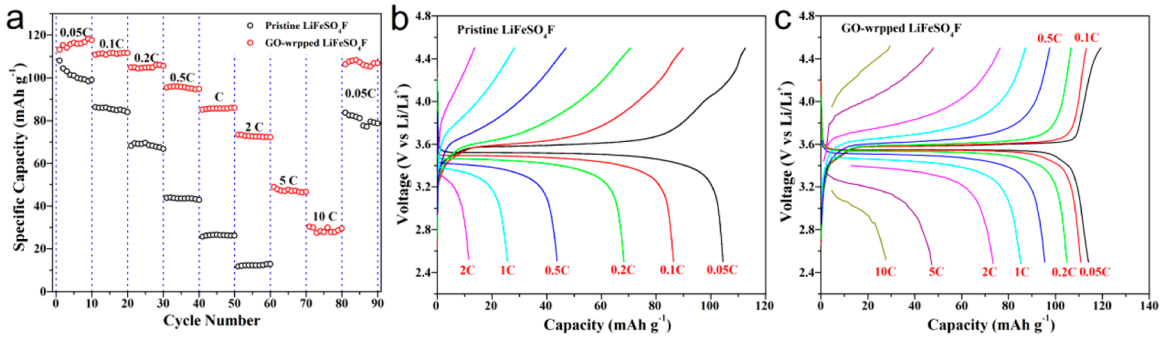

Figure 5. (a) Rate dependent cycling performance and (b, c) charge−discharge curves of the (b) pristine and (c) GO-wrapped $LiFeSO_4F$ materials at different current rates.

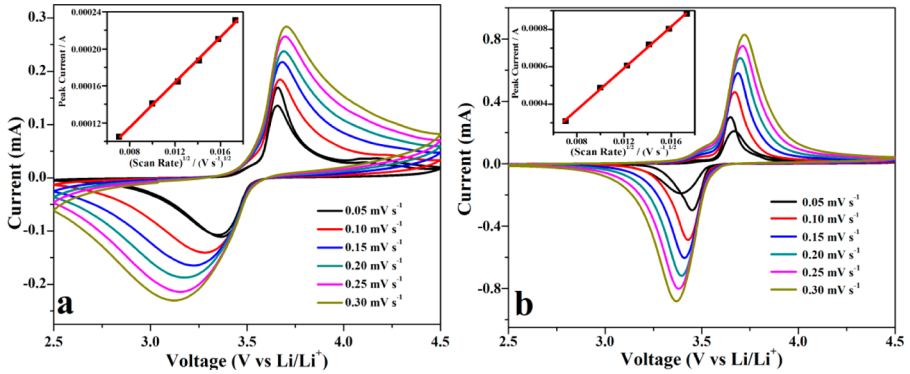

Figure 6. CV curves of (a) the pristine and (b) GO-wrapped $LiFeSO_4F$ materials at different scan rates. Inset: linear fitting of the peak current versus $(\text{scan rate})^{1/2}$.

V due to the $LiFeSO_4F/FeSO_4F$ two-phase transition.[5] The voltage gap between the charge and discharge plateaus gets smaller with GO wrapping. This indicates that the GO films can help to reduce the polarization and ohmic resistance of the batteries. In addition, it was noticed that the pristine $LiFeSO_4F$ shows a mild voltage increase at the end of the first charge, while the GO-wrapped material shows a sharp ending. This indicates fewer side reactions occurring in the GO-wrapped $LiFeSO_4F$, which will be studied in detail in the following. The initial charge−discharge capacities for the pristine $LiFeSO_4F$ are 113.0 and 99.7 mAh g^{-1}, respectively, resulting in a columbic efficiency of 88.2%. The discharge capacity of the pristine material decreases to 68.5 mAh g^{-1} after 100 cycles (Figure 4b). This indicates that some $LiFeSO_4F$ particles loss electronic contact upon cycling, possibly related to the relatively large volume change of 10.6% between the $LiFeSO_4F$ and $FeSO_4F$ phases.[29] The GO-wrapped $LiFeSO_4F$, on the contrary, shows a high initial coulombic efficiency of 97%. The discharge capacity slightly increases to 113.2 mAh g^{-1} in the initial 20 cycles. This could be due to the GO layer on the surface of the material, which blocks the Li-ion diffusion; thus, the battery needs some cycles for activation. The material shows excellent cycle stability after the activation process. A high discharge capacity of 105.6 mAh g^{-1} is obtained after 100 cycles, corresponding to capacity retention of 99% (with respect to the first cycle). This indicates that the GO films improve the cycle stability of the material due to its high flexibility, which can accommodate the volume change of $LiFeSO_4F$ during repeated charge−discharge cycling.

Figure 5, panel a shows the rate dependent cycling performance of the materials with the current rate increasing from 0.05−10 C. It was seen that the GO-wrapped $LiFeSO_4F$ always shows a higher discharge capacity compared to that of

DOI: 10.1021/acsami.5b02966
ACS Appl. Mater. Interfaces 2015, 7, 13972−13979

the pristine sample. For example, the pristine $LiFeSO_4F$ delivers a discharge capacity of 11.8 mAh g^{-1} at the 2 C rate, while the GO-wrapped $LiFeSO_4F$ exhibits a much larger discharge capacity of 73.4 mAh g^{-1}. A discharge capacity of 30.3 mAh g^{-1} can still be obtained even at the 10 C rate. In addition, the discharge capacity shows almost no fading when the current rate returns back to 0.05 C. By comparing the charge−discharge curves of the materials (Figure 5b,c), one can see that a major reason for the fast capacity fading of the pristine $LiFeSO_4F$ is its large ohmic polarizations at high current rates. This is most likely related to the poor electronic conductivity of $LiFeSO_4F$, which results in large inner resistance of the battery. In comparison, the GO-wrapped material possesses high electronic conductivity, which could reduce the ohmic polarization of the electrode thus resulting in good rate capability.

We also studied the cycling performance of the GO-wrapped $LiFeSO_4F$ with different GO amounts (Supporting Information, Figure S4). It was seen that the present material with 1.77 wt % of GO exhibits better electrochemical performance than that containing 3.89 wt % of GO. Detailed analysis of different GO-wrapped $LiFeSO_4F$ is beyond the scope of this work. However, this preliminary study shows that a small amount of GO is enough to significantly improve the electrochemical performance of $LiFeSO_4F$.

3.3. Cyclic Voltammetry. Figure 6 shows the CV curves of the pristine and GO-wrapped $LiFeSO_4F$ at different scan rates. All the CV curves are composed of a couple of cathodic/anodic peaks, which are attributed to the Li^+ extraction/insertion from the $LiFeSO_4F/FeSO_4F$ phases. Both samples maintain their symmetrical CV curves with increasing of scan rate. However, the pristine $LiFeSO_4F$ shows larger ohmic polarizations between the cathodic and anodic current peaks indicating its worse electrochemical kinetic properties. Ohmic polarization normally arises from the resistance of the electrolyte, the components of the electrode film, the current collectors, contact resistance between the active material and the conductive additive, or from a resistive solid−electrolyte interphase (SEI) film on the surface of the electrode.[30] Assuming that all the battery cells were assembled in the same way, the larger ohmic polarization of the pristine $LiFeSO_4F$ could be majorly attributed to its low electronic conductivity. In addition, it was noticed that the current flow of the GO-wrapped $LiFeSO_4F$ is much higher than that of the pristine $LiFeSO_4F$. This is also attributed to the better electrochemical kinetic properties of the material, which could result in much faster Li-ion intercalation/deintercalation. As a result, a shorter time is needed for allowing all Li ions removing from the material. Thus, the phase transformation of GO-wrapped $LiFeSO_4F$ occurs in a much narrower voltage range than that of the pristine one, as shown in the CV curves.

In addition, the current peak intensities show a linear relationship against the square root of scan rates ($v^{1/2}$) (inset of Figure 6). Therefore, the apparent lithium diffusion coefficients (D_{Li}) of the materials can be calculated by the Randles−Sevcik equation:[31]

$$I_p = 2.69 \times 10^5 A C D_{Li}^{1/2} n^{3/2} v^{1/2} \quad (1)$$

where I_p is the peak current, A is the electrode surface area, C is the concentration of Li ions in the electrode, n is the number of electrons involved in the redox process, and v is the scan rate of CV. Table 1 shows the calculated D_{Li} values of the materials in the reduction (or discharge) process. It shows that the lithium diffusion coefficient of the GO-wrapped $LiFeSO_4F$ is about 20-times larger than that of the pristine material. The lithium diffusion coefficient is a transport parameter that reflects both the ionic and the electron transports occurring in the active material. It is deduced from the Fick's first law and can be expressed as the product of a self-diffusion coefficient $D_{Li(self)}$ and a thermodynamic factor Φ, that is, $D_{Li} = D_{Li(self)} \times \Phi$. In addition, $D_{Li(self)}$ and Φ are very sensitive to the structural and electronic properties of the material, respectively. Briefly, $D_{Li(self)}$ is a measure of the diffusion that takes place even in the absence of a chemical potential gradient and corresponds to the ionic mobility or viscosity in a solution. The Φ factor measures the chemical potential deviation from that of an ideal solution. It depends on both kinetic parameters (transport number, mobility) and thermodynamic properties (stoichiometry, activity). Sometimes it indicates that the ionic flux density intensifies due to the simultaneous transport of electrons through the active material.[32−34] As an intrinsic parameter of intercalation materials, the self-diffusion coefficient of $LiFeSO_4F$ should not be changed by GO wrapping. Thus, the larger lithium diffusion coefficient of GO-wrapped $LiFeSO_4F$ should be closely related with its higher electronic conductivity. The enhancement of electronic conductivity, no matter the intrinsic electronic conductivity or the surface electronic conductivity, will lower the internal resistance of the electrode and therefore increase the internal electrical field inside the battery. As a result, the diffusion of Li ions is accelerated by this stronger internal electrical field, thus resulting in a higher lithium diffusion coefficient.

Table 1. Electrochemical Kinetic Parameters of the Pristine and GO-Wrapped $LiFeSO_4F$ Materials

	R_s (Ω)	R_f (Ω)	R_{ct} (Ω)	D_{Li} (cm^2 S^{-1})
pristine $LiFeSO_4F$	18.7	145.0	366.8	1.61×10^{-10}
GO-wrapped $LiFeSO_4F$	2.5	107.9	35.4	3.39×10^{-9}

3.4. Electrode/Electrolyte Interface Properties. As shown previously, the sharp ending of the first charge profile for the GO-wrapped $LiFeSO_4F$ indicates fewer side reactions occurring in the material. Similar to the scenario with conventional graphitic anode, the working potentials of most cathode materials used in lithium-ion batteries are too high for almost any electrolyte component to remain thermodynamically stable. Thus, the reversible Li^+ intercalation and deintercalation in cathode materials must be proceeded by complex interfacial phenomena. Side reactions and the growth of a SEI film on the electrode surface upon cycling have been evidenced for different oxide cathode materials such as $LiCoO_2$,[35] $LiNi_{0.5}Mn_{0.5}O_2$,[36] and $LiMn_2O_4$.[37] However, only little attention was paid to the electrode/electrolyte interface of polyoxyanion cathode materials because they are often considered to be more chemically inert than oxides. Recently, Aurbach et al.[38] showed that even $LiFePO_4$, which has a low voltage of 3.5 V, could react with $LiPF_6$-based electrolyte to form a SEI layer, which was further confirmed by N. Dupré et al.[39] Herein, to study the side reactions of the $LiFeSO_4F$ electrodes and the electrolyte, we carried out FTIR and TEM analyses of the electrodes before and after cycling. The cycled materials were scraped off from the electrodes after the first charge and completely washed by dimethyl carbonate (DMC) before measurements. Therefore, only solid compounds remained in the sample. Figure 7 shows the FITR spectra of

DOI: 10.1021/acsami.5b02966
ACS Appl. Mater. Interfaces 2015, 7, 13972−13979

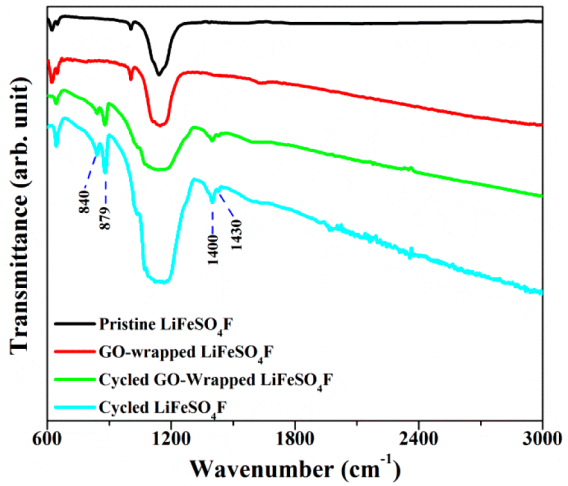

Figure 7. FITR spectra of the pristine and GO-wrapped $LiFeSO_4F$ before and after the first charge.

the pristine and GO-wrapped $LiFeSO_4F$ before and after cycling. The FTIR spectrum of the pristine and GO-wrapped $LiFeSO_4F$ fits well with that reported in literature.[40] The broad and intensive infrared (IR) peak in the wavenumber of 1114–1064 cm^{-1} is due to the asymmetrical stretching of the SO_4 tetrahedral, and the other smaller one located at 1004 cm^{-1} is due to the stretching vibration of SO_4. The typical IR peak for TEG, which should be located at 2875 cm^{-1},[41,42] is not observed, which suggests that the TEG contamination has been completely removed during the washing steps. Several new IR peaks could be observed for the cycled $LiFeSO_4F$ and GO-wrapped $LiFeSO_4F$ samples. The peak at 840 cm^{-1} is due to the P–F bond of Li_xPF_y or $Li_xPO_yF_z$,[43,44] and the peaks at 879 and 1430 cm^{-1} are assigned to the CO_3 group of Li_2CO_3.[45] In addition, the other one at 1400 cm^{-1} is assigned to the C–H vibration of carboxylic lithium compounds (RCO_2Li).[46]

The up-cutoff voltage of 4.5 V used for the $LiFeSO_4F$ electrode is too high for the $LiPF_6$-based electrolyte to maintain thermodynamic stability. According to the literature, the organic solvents in electrolyte may be decomposed at high voltage as follows:[47,48]

$$\text{EC (or DEC)} + e + Li^+ \rightarrow RCO_2Li + Li_2CO_3 \quad (1)$$

In the meantime, the $LiPF_6$ salt will decompose as follows:[49]

$$LiPF_6 \rightarrow LiF + PF_5 \quad (2)$$

$$PF_5 + H_2O \rightarrow POF_3 + 2HF \quad (3)$$

Consequently, the noxious POF_3 and HF will attack both the $LiFeSO_4F$ active material and the LiF and PF_5 byproducts, generating Li_xPF_y and $Li_xPO_yF_z$ species on the electrode surface.[50] Thus, the complex SEI mixture mainly contains Li_xPF_y, $Li_xPO_yF_z$, Li_2CO_3, and RCO_2Li, as observed by the FTIR analysis.

From the TEM image shown in Figure 8, panel a, a thick and randomly distributed SEI film could be clearly observed on the surface of $LiFeSO_4F$. In contrast, the SEI film of GO-wrapped $LiFeSO_4F$ is very uniform and much thinner than that of the pristine material. Even though the decomposition of electrolyte is unavoidable at high voltage, it is suggested that the GO can isolate the direct contact of $LiFeSO_4F$ with electrolyte, thus depressing the side reactions occurring in the battery.

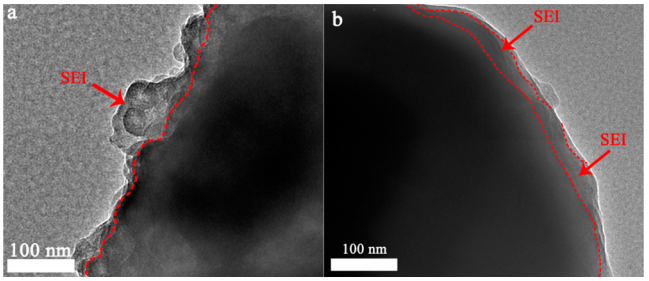

Figure 8. TEM images of the (a) pristine and (b) GO-wrapped $LiFeSO_4F$ after the first charge.

Therefore, some of the side reaction products such as Li_xPF_y and $Li_xPO_yF_z$ could be depressed by the GO. The SEI film sometimes is beneficial for electrochemical performance because it could prevent further reactions of $LiFeSO_4F$ with electrolyte. On the other hand, SEI film is a poor electronic conductor. Too thick of a SEI film on the electrode will block the transport of electrons, thus decreasing the electrochemical performance. In this regard, the GO plays important roles for the electrochemical performance of $LiFeSO_4F$ because it not only can improve the electronic conductivity of the material, but also can depress the side reactions of $LiFeSO_4F$ with electrolyte, thus resulting in a thin SEI film.

3.5. Electrochemical Impedance Spectroscopy. Finally, EIS was applied to study the effects of GO wrapping on the electrochemical kinetic properties of $LiFeSO_4F$. For the EIS measurements, the electrodes were equilibrated at the vicinity of middle point of the plateau to reach an identical status. Figure 9 shows the Nyquist plots of the materials in the first

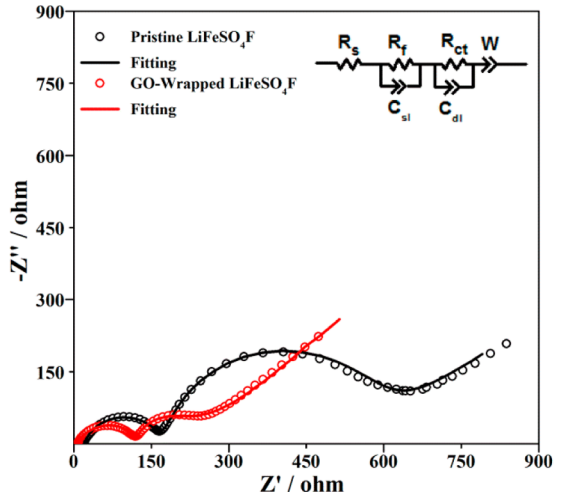

Figure 9. Nyquist plots of the pristine and GO-wrapped $LiFeSO_4F$ materials.

charge. Both electrodes show two well-defined semicircles in the high-to-middle frequency region, which are due to the SEI film and the charge transfer process, respectively. The slope line in the low frequency region is due to the lithium diffusion in the electrode bulk. On the basis of this, the Nyquist plots can be simulated by the equivalent circuit given in the inset of Figure 9. In this equivalent circuit, R_s represents the ohmic resistance of the cell. R_f and C_{sl} are the resistance and capacitance of the SEI film. R_{ct} and C_{dl} represent the charge transfer resistance and double layer capacitance. W is the

DOI: 10.1021/acsami.5b02966
ACS Appl. Mater. Interfaces 2015, 7, 13972–13979

Warburg diffusion parameter. The simulated R_s, R_f, and R_{ct} values are listed in Table 1. The GO-wrapped $LiFeSO_4F$ shows a smaller R_s value than that of pristine $LiFeSO_4F$, which indicates that the GO reduces the inner resistance of the battery. The resistance of SEI film (R_f) is also reduced by GO wrapping. As has been shown above, this could be due to the GO layers on the outer surface of $LiFeSO_4F$ that isolate the direct contact of the active material with the electrolyte, thus depressing the side reactions occurring in the battery. Most significantly, the charge transfer resistance abruptly reduces from 366.8 Ω to 35.4 Ω by GO wrapping. The improvement in charge transfer reactions could be attributed to the effective electronic conductive network constructed by the GO films, which improve the electronic distribution in the active material, thus facilitating the redox reactions and resulting in the observed excellent rate capability.

4. CONCLUSIONS

In summary, tavorite $LiFeSO_4F$ was successfully prepared by the TEG assisted solvothermal method and was further modified by GO with the assistance of APTMS. The GO intimately wraps on the surface of $LiFeSO_4F$ and effectively links the adjacent particles. This unique structure constructs an effective electronic conductive network, thus reducing the inner resistance of the battery, facilitating the charge transfer reactions at the electrode/electrolyte interface, and improving the lithium diffusion in the electrode bulk. The GO also isolates the direct contact of the active material with the electrolyte, which depresses the formation of SEI film. Because of these advantages, the GO-wrapped $LiFeSO_4F$ exhibits improved electrochemical performance such as higher specific capacities, better rate capability, and excellent capacity retention with respect to the pristine $LiFeSO_4F$.

■ ASSOCIATED CONTENT

Ⓢ Supporting Information

XRD patterns of the GO-wrapped $LiFeSO_4F$ materials with different GO amounts. Raman patterns of the pristine and GO-wrapped $LiFeSO_4F$ materials. AFM image of GO. Cycling performance of the GO-wrapped $LiFeSO_4F$ with different GO amounts at the 0.1 C rate. The Supporting Information is available free of charge on the ACS Publications website at DOI: 10.1021/acsami.5b02966.

■ AUTHOR INFORMATION

Corresponding Authors

*E-mail: yjwei@jlu.edu.cn. Phone: 86-431-85155126. Fax: 86-431-85155126.

*E-mail: dongzhang@jlu.edu.cn.

Notes

The authors declare no competing financial interest.

■ ACKNOWLEDGMENTS

This work was supported by the 973 Program of China (No. 2015CB251103), National Natural Science Foundation of China (Nos. 51472104, 51272088, 21201073), and High Technology Development Project of Jilin Province (Nos. 20150204078GX, 20150204030GX).

■ REFERENCES

(1) Masquelier, C.; Padhi, A. K.; Nanjundaswamy, K. S.; Goodenough, J. B. New Cathode Materials for Rechargeable Lithium Batteries: The 3D Framework Structures $Li_3Fe_2(XO_4)_3$ (X = P, As). *J. Solid State Chem.* **1998**, *135*, 228−234.

(2) Nyten, A.; Abouimrane, A.; Armand, M.; Gustafsson, T.; Thomas, J. O. Electrochemical Performance of Li_2FeSiO_4 as a New Li-Battery Cathode Material. *Electrochem. Commun.* **2005**, *7*, 156−160.

(3) Ellis, B. L.; Makahnouk, W. R. M.; Makimura, Y.; Toghill, K.; Nazar, L. F. A Multifunctional 3.5 V Iron-Based Phosphate Cathode for Rechargeable Batteries. *Nat. Mater.* **2007**, *6*, 749−753.

(4) Yamada, A.; Iwane, N.; Harada, Y.; Nishimura, S.-i.; Koyama, Y.; Tanaka, I. Lithium−Iron Borates as High-Capacity Battery Electrodes. *Adv. Mater.* **2010**, *22*, 3583−3587.

(5) Recham, N.; Chotard, J. N.; Dupont, L.; Delacourt, C.; Walker, W.; Armand, M.; Tarascon, J. M. A 3.6 V Lithium-Based Fluorosulphate Insertion Positive Electrode for Lithium-Ion Batteries. *Nat. Mater.* **2010**, *9*, 68−74.

(6) Frayret, C.; Villesuzanne, A.; Spaldin, N.; Bousquet, E.; Chotard, J. N.; Recham, N.; Tarascon, J. M. $LiMSO_4F$ (M = Fe, Co, and Ni): Promising New Positive Electrode Materials through the DFT Microscope. *Phys. Chem. Chem. Phys.* **2010**, *12*, 15512−15522.

(7) Tripathi, R.; Gardiner, G. R.; Islam, M. S.; Nazar, L. F. Alkali-Ion Conduction Paths in $LiFeSO_4F$ and $NaFeSO_4F$ Tavorite-Type Cathode Materials. *Chem. Mater.* **2011**, *23*, 2278−2284.

(8) Lee, S.; Park, S. S. Comparative Study of Tavorite and Triplite $LiFeSO_4F$ as Cathode Materials for Lithium Ion Batteries: Structure, Defect Chemistry, and Lithium Conduction Properties from Atomistic Simulation. *J. Phys. Chem. C* **2014**, *118*, 12642−12648.

(9) Amin, R.; Balaya, P.; Maier, J. Anisotropy of Electronic and Ionic Transport in $LiFePO_4$ Single Crystals. *Electrochem. Solid State Lett.* **2007**, *10*, A13−A16.

(10) Yang, S. L.; Wang, L. P.; Ma, R. G.; Lu, Z. G.; Xi, L. J.; Hu, M. J.; Dong, Y. C.; Chung, C. Y. Triethylene Glycol Assisted Synthesis of Pure Tavorite $LiFeSO_4F$ Cathode Material for Li-Ion Battery. *J. Electrochem. Soc.* **2013**, *160*, A3072−A3076.

(11) Tripathi, R.; Ramesh, T. N.; Ellis, B. L.; Nazar, L. F. Scalable Synthesis of Tavorite $LiFeSO_4F$ and $NaFeSO_4F$ Cathode Materials. *Angew. Chem., Int. Ed.* **2010**, *49*, 8738−8742.

(12) Sobkowiak, A.; Roberts, M. R.; Younesi, R.; Ericsson, T.; Haggstrom, L.; Tai, C. W.; Anderssor, A. M.; Edstrom, K.; Gustafsson, T.; Bjorefors, F. Understanding and Controlling the Surface Chemistry of $LiFeSO_4F$ for an Enhanced Cathode Functionality. *Chem. Mater.* **2013**, *25*, 3020−3029.

(13) Dan Thien, N.; Cao Cuong, N.; Kim, J. S.; Kim, J. Y.; Song, S. W. Facile Synthesis and High Anode Performance of Carbon Fiber-Interwoven Amorphous Nano-SiO_x/Graphene for Rechargeable Lithium Batteries. *ACS Appl. Mater. Interfaces* **2013**, *5*, 11234−11239.

(14) Elazari, R.; Salitra, G.; Garsuch, A.; Panchenko, A.; Aurbach, D. Sulfur-Impregnated Activated Carbon Fiber Cloth as a Binder-Free Cathode for Rechargeable Li−S Batteries. *Adv. Mater.* **2011**, *23*, 5641−5644.

(15) Zhou, J.; Zhang, D.; Zhang, X.; Song, H.; Chen, X. Carbon-Nanotube-Encapsulated FeF_2 Nanorods for High-Performance Lithium-Ion Cathode Materials. *ACS Appl. Mater. Interfaces* **2014**, *6*, 21223−21229.

(16) Zhai, C.; Du, N.; Zhang, H.; Yu, J.; Yang, D. Multiwalled Carbon Nanotubes Anchored with SnS_2 Nanosheets as High-Performance Anode Materials of Lithium-Ion Batteries. *ACS Appl. Mater. Interfaces* **2011**, *3*, 4067−4074.

(17) Guo, J.; Xu, Y.; Wang, C. Sulfur-Impregnated Disordered Carbon Nanotubes Cathode for Lithium−Sulfur Batteries. *Nano Lett.* **2011**, *11*, 4288−4294.

(18) Zhou, X.; Wan, L. J.; Guo, Y. G. Facile Synthesis of MoS_2@CMK-3 Nanocomposite as an Improved Anode Material for Lithium-Ion Batteries. *Nanoscale* **2012**, *4*, 5868−5871.

(19) Tao, X.; Chen, X.; Xia, Y.; Huang, H.; Gan, Y.; Wu, R.; Chen, F.; Zhang, W. Highly Mesoporous Carbon Foams Synthesized by a Facile, Cost-Effective, and Template-Free Pechini Method for Advanced Lithium−Sulfur Batteries. *J. Mater. Chem. A* **2013**, *1*, 3295−3301.

DOI: 10.1021/acsami.5b02966
ACS Appl. Mater. Interfaces 2015, 7, 13972−13979

(20) Fang, X.; Ge, M.; Rong, J.; Zhou, C. Graphene-Oxide-Coated $LiNi_{0.5}Mn_{1.5}O_4$ as High Voltage Cathode for Lithium-Ion Batteries with High Energy Density and Long Cycle Life. *J. Mater. Chem. A* **2013**, *1*, 4083−4088.
(21) Wang, K.; Wang, Y.; Wang, C.; Xia, Y. Graphene Oxide Assisted Solvothermal Synthesis of $LiMnPO_4$ Naonplates Cathode Materials for Lithium-Ion Batteries. *Electrochim. Acta* **2014**, *146*, 8−14.
(22) Zhou, G.; Wang, D. W.; Li, F.; Zhang, L.; Li, N.; Wu, Z. S.; Wen, L.; Lu, G. Q.; Cheng, H. M. Graphene-Wrapped Fe_3O_4 Anode Material with Improved Reversible Capacity and Cyclic Stability for Lithium-Ion Batteries. *Chem. Mater.* **2010**, *22*, 5306−5313.
(23) Hummers, W. S.; Offeman, R. E. Preparation of Graphitic Oxide. *J. Am. Chem. Soc.* **1958**, *80*, 1339−1339.
(24) Wang, H.; Hao, Q.; Yang, X.; Lu, L.; Wang, X. Graphene Oxide Doped Polyaniline for Supercapacitors. *Electrochem. Commun.* **2009**, *11*, 1158−1161.
(25) Liang, C.; Zhai, T.; Wang, W.; Chen, J.; Zhao, W.; Lu, X.; Tong, Y. Fe_3O_4/Reduced Graphene Oxide with Enhanced Electrochemical Performance Towards Lithium Storage. *J. Mater. Chem. A* **2014**, *2*, 7214−7220.
(26) Yan, X.; Li, Y.; Du, F.; Zhu, K.; Zhang, Y.; Su, A.; Chen, G.; Wei, Y. Synthesis and Optimizable Electrochemical Performance of Reduced Graphene Oxide Wrapped Mesoporous TiO_2 Microspheres. *Nanoscale* **2014**, *6*, 4108−4116.
(27) Ramana, C. V.; Ait-Salah, A.; Utsunomiya, S.; Morhange, J. F.; Mauger, A.; Gendron, F.; Julien, C. M. Spectroscopic and Chemical Imaging Analysis of Lithium Iron Triphosphate. *J. Phys. Chem. C* **2006**, *111*, 1049−1054.
(28) Zhu, X.; Hu, J.; Wu, W.; Zeng, W.; Dai, H.; Du, Y.; Liu, Z.; Li, L.; Ji, H.; Zhu, Y. $LiFePO_4$/Reduced Graphene Oxide Hybrid Cathode for Lithium-Ion Battery with Outstanding Rate Performance. *J. Mater. Chem. A* **2014**, *2*, 7812−7818.
(29) Ati, M.; Melot, B. C.; Chotard, J. N.; Rousse, G.; Reynaud, M.; Tarascon, J. M. Synthesis and Electrochemical Properties of Pure $LiFeSO_4F$ in the Triplite Structure. *Electrochem. Commun.* **2011**, *13*, 1280−1283.
(30) Winter, M.; Brodd, R. J. What Are Batteries, Fuel Cells, and Supercapacitors? *Chem. Rev.* **2004**, *104*, 4245−4269.
(31) Jiang, T.; Pan, W.; Wang, J.; Bie, X.; Du, F.; Wei, Y.; Wang, C.; Chen, G. Carbon Coated $Li_3V_2(PO_4)_3$ Cathode Material Prepared by a PVA Assisted Sol−Gel Method. *Electrochim. Acta* **2010**, *55*, 3864−3869.
(32) Wagner, C. Investigations on Silver Sulfide. *J. Chem. Phys.* **1953**, *21*, 1819−1827.
(33) Bruce, P. G. *Solid State Electrochemistry*; Cambridge University Press: Cambridge, 1995; Vol. 5.
(34) Montoro, L. A.; Matsubara, E. Y.; Rosolen, J. M. Lithium Intercalation into Single-Walled Carbon Nanotubes Network Electrode: Storage Mechanisms and Impurity Effects. *J. Power Sources* **2014**, *257*, 205−212.
(35) Matsuta, S.; Kato, Y.; Ota, T.; Kurokawa, H.; Yoshimura, S.; Fujitani, S. Electron-Spin-Resonance Study of the Reaction of Electrolytic Solutions on the Positive Electrode for Lithium-Ion Secondary Batteries. *J. Electrochem. Soc.* **2001**, *148*, A7−A10.
(36) Dupré, N.; Martin, J.-F.; Oliveri, J.; Soudan, P.; Guyomard, D.; Yamada, A.; Kanno, R. Aging of the $LiNi_{1/2}Mn_{1/2}O_2$ Positive Electrode Interface in Electrolyte. *J. Electrochem. Soc.* **2009**, *156*, C180−C185.
(37) Yang, L.; Ravdel, B.; Lucht, B. L. Electrolyte Reactions with the Surface of High Voltage $LiNi_{0.5}Mn_{1.5}O_4$ Cathodes for Lithium-Ion Batteries. *Electrochem. Solid State Lett.* **2010**, *13*, A95−A97.
(38) Koltypin, M.; Aurbach, D.; Nazar, L.; Ellis, B. More on the Performance of $LiFePO_4$ Electrodes—The Effect of Synthesis Route, Solution Composition, Aging, and Temperature. *J. Power Sources* **2007**, *174*, 1241−1250.
(39) Dupré, N.; Martin, J. F.; Degryse, J.; Fernandez, V.; Soudan, P.; Guyomard, D. Aging of the $LiFePO_4$ Positive Electrode Interface in Electrolyte. *J. Power Sources* **2010**, *195*, 7415−7425.
(40) Radha, A. V.; Furman, J. D.; Ati, M.; Melot, B. C.; Tarascon, J. M.; Navrotsky, A. Understanding the Stability of Fluorosulfate Li-Ion Battery Cathode Materials: A Thermochemical Study of $LiFe_{1-x}Mn_xSO_4F$ ($0 \le x \le 1$) Polymorphs. *J. Mater. Chem.* **2012**, *22*, 24446−24452.
(41) Recham, N.; Rousse, G.; Sougrati, M. T.; Chotard, J. N.; Frayret, C.; Mariyappan, S.; Melot, B. C.; Jumas, J. C.; Tarascon, J. M. Preparation and Characterization of a Stable $FeSO_4F$-Based Framework for Alkali Ion Insertion Electrodes. *Chem. Mater.* **2012**, *24*, 4363−4370.
(42) Azib, T.; Ammar, S.; Nowak, S.; Lau Truing, S.; Groult, H.; Zaghib, K.; Mauger, A.; Julien, C. M. Crystallinity of Nano C-$LiFePO_4$ Prepared by the Polyol Process. *J. Power Sources* **2012**, *217*, 220−228.
(43) Koltypin, M.; Aurbach, D.; Nazar, L.; Ellis, B. On the Stability of $LiFePO_4$ Olivine Cathodes under Various Conditions (Electrolyte Solutions, Temperatures). *Electrochem. Solid State Lett.* **2007**, *10*, A40−A44.
(44) Aurbach, D.; Gamolsky, K.; Markovsky, B.; Salitra, G.; Gofer, Y.; Heider, U.; Oesten, R.; Schmidt, M. The Study of Surface Phenomena Related to Electrochemical Lithium Intercalation into Li_xMO_y Host Materials (M = Ni, Mn). *J. Electrochem. Soc.* **2000**, *147*, 1322−1331.
(45) Aurbach, D.; Gofer, Y.; Ben-Zion, M.; Aped, P. The Behavior of Lithium Electrodes in Propylene and Ethylene Carbonate: The Major Factors That Influence Li Cycling Efficiency. *J. Electroanal. Chem.* **1992**, *339*, 451−471.
(46) Wang, Z.; Sun, Y.; Chen, L.; Huang, X. Electrochemical Characterization of Positive Electrode Material $LiNi_{1/3}Co_{1/3}Mn_{1/3}O_2$ and Compatibility with Electrolyte for Lithium-Ion Batteries. *J. Electrochem. Soc.* **2004**, *151*, A914−A921.
(47) Aurbach, D.; Gamolsky, K.; Markovsky, B.; Salitra, G.; Gofer, Y.; Heider, U.; Oesten, R.; Schmidt, M. The Study of Surface Phenomena Related to Electrochemical Lithium Intercalation into Li_xMO_y Host Materials (M = Ni, Mn). *J. Electrochem. Soc.* **2000**, *147*, 1322−1331.
(48) Shin, J. S.; Han, C. H.; Jung, U. H.; Lee, S. I.; Kim, H. J.; Kim, K. Effect of Li_2CO_3 Additive on Gas Generation in Lithium-Ion Batteries. *J. Power Sources* **2002**, *109*, 47−52.
(49) Edström, K.; Gustafsson, T.; Thomas, J. O. The Cathode−Electrolyte Interface in the Li-Ion Battery. *Electrochim. Acta* **2004**, *50*, 397−403.
(50) Jo, C. H.; Cho, D. H.; Noh, H. J.; Yashiro, H.; Sun, Y. K.; Myung, S. An Effective Method To Reduce Residual Lithium Compounds on Ni-Rich $Li[Ni_{0.6}Co_{0.2}Mn_{0.2}]O_2$ Active Material Using a Phosphoric Acid Derived Li_3PO_4 Nanolayer. *Nano Res.* **2015**, *8*, 1464−1479.

DOI: 10.1021/acsami.5b02966
ACS Appl. Mater. Interfaces 2015, 7, 13972−13979